Progress In Electromagnetics Research C, Vol. 82, 209–223, 2018

Analysis of Field Propagation through a Multiport Frequency Selective Network Using Cavity Modeling Technique

Ashmi C. Das and Santanu Dwari*

Abstract—This paper presents the applicability of cavity modeling technique to analyze field propagation inside a multiport waveguide network. For a better understanding of the subject, we have considered a five-port quadraplexer as our target network. Field propagations within the network at different passband and stopband frequencies have been presented. The analysis has been verified by comparing the overall frequency response of the network with the available data in literature. The analysis demonstrates the field division at different junctions as well as field attenuation/propagation at different points of the network, which will be helpful for designing more complex and/or advanced multiport waveguide networks. It also demonstrates the presence of higher order modes at different discontinuities of the network and their effects on the respective field distributions.

1. INTRODUCTION

A survey of literature in last one and half decade on different rectangular waveguide based networks and aperture antennas reveals that cavity modeling technique has been extensively used to analyze them [1–6]. The technique was initially proposed by Vengadarajan in his PhD thesis "Multiple Cavity Modeling Technique for Solving Aperture Coupled Waveguide Junctions" [7]. Later, Das, Panda and Gayen extended his work in different aspects. In 2006, Das and Chakraborty first demonstrated the cavity modeling technique in open literature by analyzing some simple waveguide structures such as dielectric plug loaded open ended waveguide in transmit and receiving mode, waveguide step discontinuity, and even-odd mode analysis of interacting identical inductive diaphragm in a waveguide [1]. Next year they analyzed a broad wall longitudinal/transverse slot coupled crossed waveguide junction considering the TE_{00} mode at the slot aperture [2]. Two years later, Das and Chakraborty applied the cavity modeling technique on a simple but electrically large structures (waveguide taper and horn antenna) to test its applicability in analyzing electrically large structures [3]. They pointed out the limitations of cavity modeling technique in analyzing the electrically large structures using the example of a 7-inch square horn. In 2008, Panda and Chakraborty, used cavity modeling technique to analyze a $1:3$ H-plane power divider, loaded with a rectangular shorting post [4]. In the same year they analyzed the co-channel interference in a two-channel waveguide joint. In 2013, Gayen and Das presented cavity model based analysis of a high-gain broad-band waveguide longitudinal slot array antenna [6]. In all these analyses emphasis was given on finding scattering characteristics of the networks. Aperture field distribution at the joints and different apertures of the networks, which give a detail insight of the operation of the network, were not studied properly. Further the structures that were analyzed by them are very simple in nature. A test of cavity modeling technique in analyzing a complicated network, such as multiport frequency selective network, remained untouched.

Received 8 January 2018, Accepted 8 March 2018, Scheduled 3 April 2018
* Corresponding author: Santanu Dwari (sdwari@gmail.com).
The authors are with the Department of Electronics Engineering, Indian Institute of Technology (Indian School of Mines), Dhanbad, India.

Cavity model analysis of a network involves modeling of the network using rectangular cavities and replacement of the electric fields at the apertures and discontinuities with equivalent magnetic current densities. In general, multiple cavities are required to model a network, and therefore, the technique is also called multiple cavity modeling technique (MCMT). The advantage of the technique is that very few meshes (or cavities) are required for the analysis of the network instead of thousands of meshes done in a commercial electromagnetic software. This can make the simulation of the structure very fast. On the negative side, the technique is not fully tested and has limited applicability. The structures that have been analyzed using cavity modeling technique are symmetric and asymmetric power dividers, T-junctions, and different kinds of radiators (e.g., open ended waveguide and slot radiator). On the application side, they have been used to do even and odd mode analysis of symmetric network, estimate EMI from faulty joints/cracks, and analyze the effects of imperfect termination.

A comparison of the results obtained using the cavity modeling technique with measured or simulated data obtained using commercial electromagnetic software, as published in the literatures, reveals that they are very close. So the cavity modeling technique has the potential to become a numerical tool that can be used to analyze a rectangular waveguide based network in absence of the costly commercially available software/measurement setups. Therefore, in this work an attempt has been made to extend the applicability of cavity modeling technique to study field propagation in a complex, frequency dependent multiport network and to study the presence and effects of higher order modes at the apertures/junctions/discontinuities in terms of aperture field distribution. To do this the quadraplexer, presented in [8], has been taken as target network. The modeling of the quadraplexer requires thirty six cavities, five waveguide regions (or ports) and forty apertures, which is maximum among any structures available in the literature which have been analyzed using cavity modeling technique. Being a frequency dependent structure it also involves a frequency dependent field propagation among the ports, which can be a real test of the cavity modeling technique.

2. CAVITY MODEL ANALYSIS

The cut plane view of the proposed quadraplexer is shown in Fig. 1(a) whereas its cavity modeling is shown in Fig. 1(b). In the figure, the waveguide sections (W_1–W_5) represent the ports, with W_1 being the input port and W_2–W_5 the output ports. The network has been modelled using thirty six cavities (C_1–C_{36}), which create forty apertures between different regions. The electric field at the apertures

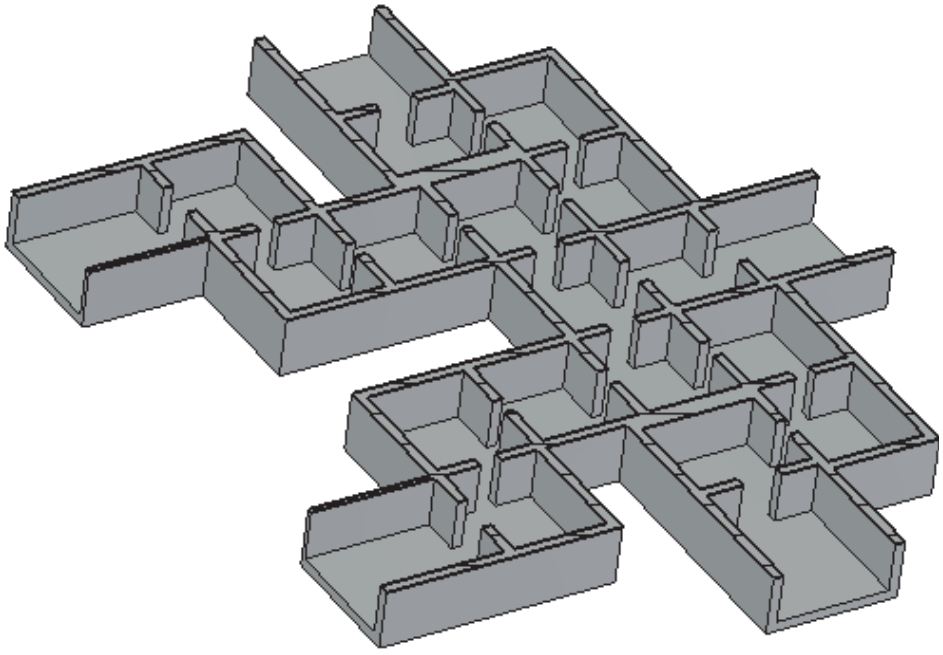

(a)

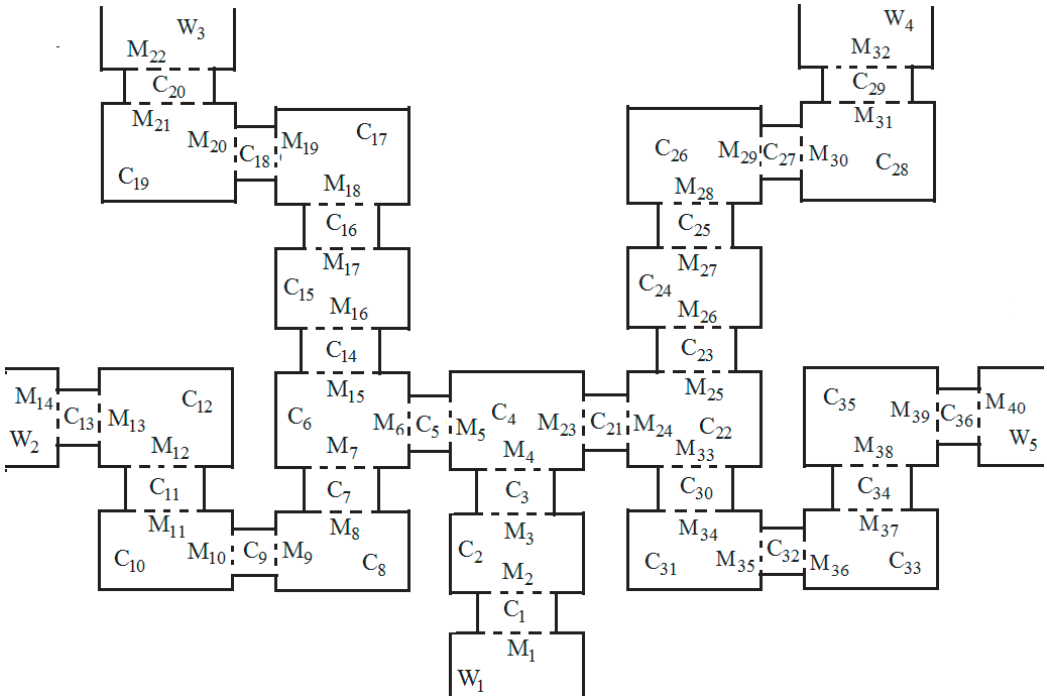

Figure 1. Quadraplexer circuit, (a) cut-plane view and (b) cavity modeling (top view/XZ plane).

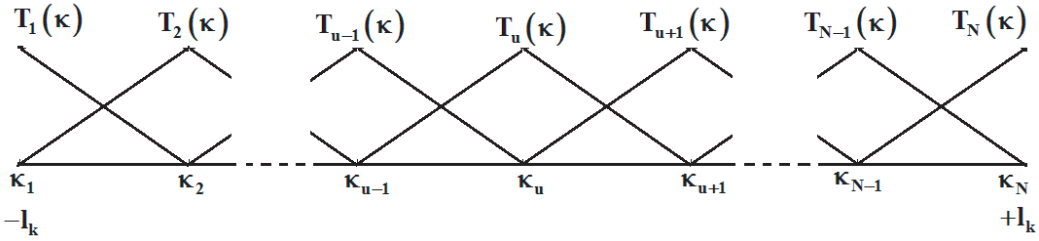

Figure 2. Triangular basis function.

has been represented in terms of equivalent magnetic current densities (M_1–M_{40}) by using equivalence principle. The aperture electric field/equivalent magnetic current is unknown, but can be represented by a two-dimensional weighted triangular basis function as shown in Fig. 2 and represented by Equation (1).

$$M_i^{\xi/y} = \sum_{p,q=1}^{N} E_{p,q}^{i,\xi/y} T_p(\xi)\, T_q(y) \tag{1}$$

where (ξ, y) defines the plane of the aperture, and (p, q) are the numbers of corresponding basis functions. $T_u(\kappa)$ $(u = p/q)$, $E_{p,q}^{i,\xi/y}$ are the unknown weights of the basis function and

$$T_u(\kappa) = \begin{cases} \dfrac{\kappa - \kappa_{u-1}}{\kappa_u - \kappa_{u-1}} & \text{for} \quad \kappa_{u-1} \le \kappa \le \kappa_u \\ \dfrac{\kappa_{u+1} - \kappa}{\kappa_{u+1} - \kappa_u} & \text{for} \quad \kappa_u \le \kappa \le \kappa_{u+1} \end{cases} \qquad u = p/q \text{ and } \kappa = \xi/y \tag{2}$$

To determine the unknown weights $E_{p,q}^{i,\xi/y}$ and hence the aperture field (or equivalent magnetic currents), we need to find and solve the boundary conditions. The boundary conditions can be found

by equating the tangential component of magnetic fields at each region, across the boundary. The net tangential magnetic field in a particular region can be found by using superposition principle. For example, there are six sources in $C_4(M_4^x,\, M_4^y,\, M_5^z,\, M_5^y,\, -M_{23}^z$ and $-M_{23}^y)$, and four sources in C_3 $(M_3^x,\, M_3^y,\, -M_4^x$ and $-M_4^y)$. So the net tangential fields on aperture 4 in both regions will be
Cavity 3:

$$H_x^{c\_3}\left(M_3^x\right)+H_x^{c\_3}\left(M_3^y\right)+H_x^{c\_3}\left(-M_4^x\right)+H_x^{c\_3}\left(-M_4^y\right)$$
$$H_y^{c\_3}\left(M_3^x\right)+H_y^{c\_3}\left(M_3^y\right)+H_y^{c\_3}\left(-M_4^x\right)+H_y^{c\_3}\left(-M_4^y\right)$$

Cavity 4:

$$H_x^{c\_4}\left(M_4^x\right)+H_x^{c\_4}\left(M_4^y\right)+H_x^{c\_4}\left(M_5^z\right)+H_x^{c\_4}\left(M_5^y\right)+H_x^{c\_4}\left(-M_{23}^z\right)+H_x^{c\_4}\left(-M_{23}^y\right)$$
$$H_y^{c\_4}\left(M_4^x\right)+H_y^{c\_4}\left(M_4^y\right)+H_y^{c\_4}\left(M_5^z\right)+H_y^{c\_4}\left(M_5^y\right)+H_y^{c\_4}\left(-M_{23}^z\right)+H_y^{c\_4}\left(-M_{23}^y\right)$$

and the boundary conditions can be derived as

$$\begin{aligned}&-H_x^{c\_3}\left(M_3^x\right)-H_x^{c\_3}\left(M_3^y\right)+H_x^{c\_3}\left(M_4^x\right)+H_x^{c\_4}\left(M_4^x\right)+H_x^{c\_3}\left(M_4^y\right)+H_x^{c\_4}\left(M_4^y\right)\\&+H_x^{c\_4}\left(M_5^z\right)+H_x^{c\_4}\left(M_5^y\right)-H_x^{c\_4}\left(M_{23}^z\right)-H_x^{c\_4}\left(M_{23}^y\right)=0\end{aligned}\tag{3}$$

$$\begin{aligned}&-H_y^{c\_3}\left(M_3^x\right)-H_y^{c\_3}\left(M_3^y\right)+H_y^{c\_3}\left(M_4^x\right)+H_y^{c\_4}\left(M_4^x\right)+H_y^{c\_3}\left(M_4^y\right)+H_y^{c\_4}\left(M_4^y\right)\\&+H_y^{c\_4}\left(M_5^z\right)+H_y^{c\_4}\left(M_5^y\right)-H_y^{c\_4}\left(M_{23}^z\right)-H_y^{c\_4}\left(M_{23}^y\right)=0\end{aligned}\tag{4}$$

The tangential magnetic fields in different regions can be derived from aperture field distribution using Green's function approach [1] (for cavity regions) or modal expansion method [9] (for waveguide regions). Doing so, tangential components of magnetic fields in cavity and waveguide regions can be derived as

$$H_\xi^{c\_v}\left(M_i^\xi\right)=\frac{j\omega\varepsilon}{k^2}\sum_{m=1}^{\infty}\sum_{n=0}^{\infty}\frac{\varepsilon_m\varepsilon_n}{4l_\xi l_y}\left\{k^2-\left(\frac{m\pi}{2l_\xi}\right)^2\right\}\sin\left\{\frac{m\pi}{2l_\xi}\left(\xi+l_\xi\right)\right\}\cos\left\{\frac{n\pi}{2l_y}\left(y+l_y\right)\right\}$$
$$\frac{TRIA\xi\xi\left(p,m\right)TRIA\xi Y\left(q,n\right)}{\Gamma_{mn\chi}\sin\left(2\Gamma_{mn\chi}\chi\right)}\begin{cases}\cos\left\{\Gamma_{mn\chi}\left(\chi-l_\chi\right)\right\}\cos\left\{\Gamma_{mn\chi}\left(\chi'+l_\chi\right)\right\} & \text{for}\quad \chi{>}\chi'\\ \cos\left\{\Gamma_{mn\chi}\left(\chi'-l_\chi\right)\right\}\cos\left\{\Gamma_{mn\chi}\left(\chi+l_\chi\right)\right\} & \text{for}\quad \chi<\chi'\end{cases}\tag{5}$$

$$H_\xi^{c\_v}\left(M_i^y\right)=-\frac{j\omega\varepsilon}{k^2}\sum_{m=0}^{\infty}\sum_{n=1}^{\infty}\frac{\varepsilon_m\varepsilon_n}{4l_\xi l_y}\frac{m\pi}{2l_\xi}\frac{n\pi}{2l_y}\sin\left\{\frac{m\pi}{2l_\xi}\left(\xi+l_\xi\right)\right\}\cos\left\{\frac{n\pi}{2l_y}\left(Y+l_y\right)\right\}$$
$$\frac{TRIAY\xi\left(p,m\right)TRIAYY\left(q,n\right)}{\Gamma_{mn\chi}\sin\left(2\Gamma_{mn\chi}\chi\right)}\begin{cases}\cos\left\{\Gamma_{mn\chi}\left(\chi-l_\chi\right)\right\}\cos\left\{\Gamma_{mn\chi}\left(\chi'+l_\chi\right)\right\} & \text{for}\quad \chi{>}\chi'\\ \cos\left\{\Gamma_{mn\chi}\left(\chi'-l_\chi\right)\right\}\cos\left\{\Gamma_{mn\chi}\left(\chi+l_\chi\right)\right\} & \text{for}\quad \chi<\chi'\end{cases}\tag{6}$$

$$H_y^{c\_v}\left(M_i^\xi\right)=-\frac{j\omega\varepsilon}{k^2}\sum_{m=1}^{\infty}\sum_{n=0}^{\infty}\frac{\varepsilon_m\varepsilon_n}{4l_\xi l_y}\frac{m\pi}{2l_\xi}\frac{n\pi}{2l_y}\cos\left\{\frac{m\pi}{2l_\xi}\left(\xi+l_\xi\right)\right\}\sin\left\{\frac{n\pi}{2l_y}\left(\zeta+l_y\right)\right\}$$
$$\frac{TRIA\xi\xi\left(p,m\right)TRIA\xi Y\left(q,n\right)}{\Gamma_{mn\chi}\sin\left(2\Gamma_{mn\chi}\chi\right)}\begin{cases}\cos\left\{\Gamma_{mn\chi}\left(\chi-l_\chi\right)\right\}\cos\left\{\Gamma_{mn\chi}\left(\chi'+l_\chi\right)\right\} & \text{for}\quad \chi{>}\chi'\\ \cos\left\{\Gamma_{mn\chi}\left(\chi'-l_\chi\right)\right\}\cos\left\{\Gamma_{mn\chi}\left(\chi+l_\chi\right)\right\} & \text{for}\quad \chi<\chi'\end{cases}\tag{7}$$

$$H_y^{c\_v}\left(M_i^y\right)=\frac{j\omega\varepsilon}{k^2}\sum_{m=0}^{\infty}\sum_{n=1}^{\infty}\frac{\varepsilon_m\varepsilon_n}{4l_\xi l_y}\left\{k^2-\left(\frac{n\pi}{2l_y}\right)^2\right\}\cos\left\{\frac{m\pi}{2l_\xi}\left(\xi+l_\xi\right)\right\}\sin\left\{\frac{n\pi}{2l_y}\left(\zeta+l_y\right)\right\}$$
$$\frac{TRIAY\xi\left(p,m\right)TRIAYY\left(q,n\right)}{\Gamma_{mn\chi}\sin\left(2\Gamma_{mn\chi}\chi\right)}\begin{cases}\cos\left\{\Gamma_{mn\chi}\left(\chi-l_\chi\right)\right\}\cos\left\{\Gamma_{mn\chi}\left(\chi'+l_\chi\right)\right\} & \text{for}\quad \chi{>}\chi'\\ \cos\left\{\Gamma_{mn\chi}\left(\chi'-l_\chi\right)\right\}\cos\left\{\Gamma_{mn\chi}\left(\chi+l_\chi\right)\right\} & \text{for}\quad \chi<\chi'\end{cases}\tag{8}$$

$$H_\xi^{w\_v}\left(M_i^\xi\right)=-\sum_{m=1}^{\infty}\sum_{n=0}^{\infty}\left\{Y_{mn}^e\left(C_{mn}^e\frac{m\pi}{2a}\right)^2+Y_{mn}^m\left(C_{mn}^m\frac{n\pi}{2b}\right)^2\right\}\sin\left\{\frac{m\pi}{2a}\left(\xi{+}a\right)\right\}\cos\left\{\frac{n\pi}{2b}\left(y{+}b\right)\right\}$$
$$TRIA\xi\xi\left(p,m\right)TRIA\xi Y\left(q,n\right)\tag{9}$$

$$H_\xi^{w\_v}\left(M_i^y\right)=-\sum_{m=0}^{\infty}\sum_{n=1}^{\infty}\left\{Y_{mn}^e\left(C_{mn}^e\right)^2{-}Y_{mn}^m\left(C_{mn}^m\right)^2\right\}\frac{m\pi}{2a}\frac{n\pi}{2b}\sin\left\{\frac{m\pi}{2a}\left(\xi{+}a\right)\right\}\cos\left\{\frac{n\pi}{2b}\left(y{+}b\right)\right\}$$
$$TRIAY\xi\left(p,m\right)TRIAYY\left(q,n\right)\tag{10}$$

where $2a$ and $2b$ are the width and height of the waveguide; (m, n) represent particular modes; (l_ξ, l_y, l_χ) are the dimensions of cavity along (ξ, Y, χ) direction; (ξ, Y) represents the plane of the aperture; χ is the direction of propagation (or normal of the plane of the aperture) and

$$C^e_{mn} = \frac{1}{\pi}\sqrt{\frac{ab\varepsilon_m\varepsilon_n}{(mb)^2+(na)^2}} \tag{11}$$

$$C^m_{mn} = \frac{2}{\pi}\sqrt{\frac{ab}{(mb)^2+(na)^2}} \tag{12}$$

$$TRIA\xi\xi\,(p,m) = \int_{\xi_{u-1}}^{\xi_{u+1}} \sin\left\{\frac{m\pi}{2l_\xi}(\xi+l_\xi)\right\} T_p(\xi)\,d\xi \tag{13}$$

$$TRIAY\xi\,(p,m) = \int_{\xi_{u-1}}^{\xi_{u+1}} \cos\left\{\frac{m\pi}{2l_\xi}(\xi+l_\xi)\right\} T_p(\xi)\,d\xi \tag{14}$$

$$TRIA\xi Y\,(q,n) = \int_{y_{u-1}}^{y_{u+1}} \cos\left\{\frac{n\pi}{2l_y}(y+l_y)\right\} T_q(y)\,dy \tag{15}$$

$$TRIAYY\,(q,n) = \int_{y_{u-1}}^{y_{u+1}} \sin\left\{\frac{n\pi}{2l_y}(y+l_y)\right\} T_q(y)\,dy \tag{16}$$

ε_m and ε_n are Neumann's function. During derivation of the integration of Eqs. (13)–(16), it may be noted that for $u = 1$ there will be only falling edge whereas for $u = N$ there will be only rising edge of the triangular basis function, as shown in Fig. 2. The excitation field can be assumed as dominant TE_{10} mode and expressed as,

$$H^{inc}_x = -Y_0 \cos\left(\frac{\pi x}{2a}\right) e^{-j\beta z} \tag{17}$$

Since there are total forty apertures, and each aperture has two boundary conditions, corresponding to the two tangential components, total eighty boundary equations will be obtained for the quadraplexer. The solution of the eighty simultaneous boundary conditions using Galerkins specialization of method of moment will provide values of the unknown weights. Once the weights have been found, the electric field distributions (or equivalent magnetic current densities) on the apertures can be determined using Equation (1).

To verify the analysis, the dominant mode reflection and transmission coefficients of the network have been found using the following equations:

$$\Gamma = -1 + \frac{1}{2ab}Y_{10}\sum_{p,\,q=1}^{N} E^{s,\xi}_{p,q}\, TRIA\xi\xi\,(p)|_{m=1}\, TRIA\xi Y\,(q)|_{n=0} \tag{18}$$

$$\mathrm{T} = \frac{1}{2ab}Y_{10}\sum_{p,\,q=1}^{N} E^{o,\xi}_{p,q}\, TRIA\xi\xi\,(p)|_{m=1}\, TRIA\xi Y\,(q)|_{n=0} \tag{19}$$

and compared with the literature available data [8]. In Equations (18)–(19), "s" represents the input port aperture, and "o" represents the output port aperture.

3. RESULTS AND DISCUSSION

The aperture field distributions on the input-output ports and on different apertures and junctions of the quadraplexer are shown in Figs. 3–7 for 9.895, 9.97, 10, 10.035 and 10.11 GHz, respectively.

Figs. 3(a)–3(c) reveal that at 9.895 GHz the incident field propagates from the input port to cavity 4 where it is channeled towards cavity 5 through aperture 5 and cavity 21 through aperture 23. Further observations on Figs. 3(d)–(g) reveal that the field coupled to cavity 6 through apertures 5 and 6 is routed towards port 2 rather than port 4. Therefore, we get a passband at port 2 and stopband at port 3. The propagation of field from aperture 23 towards ports 4 and 5 is shown in Figs. 3(h)–3(l), which reveals stopbands at both ports 4 and 5. A similar observations of Figs. 4, 6–7 reveals that we get passband at port 3 and stopband at other output ports at 9.97 GHz; passband at port 4 and stopband at other output ports at 10.035 GHz; passband at port 5 and stopband at other output ports at 10.11 GHz. Fig. 5 reveals that fields at all the output ports are negligible, which implies stopband at

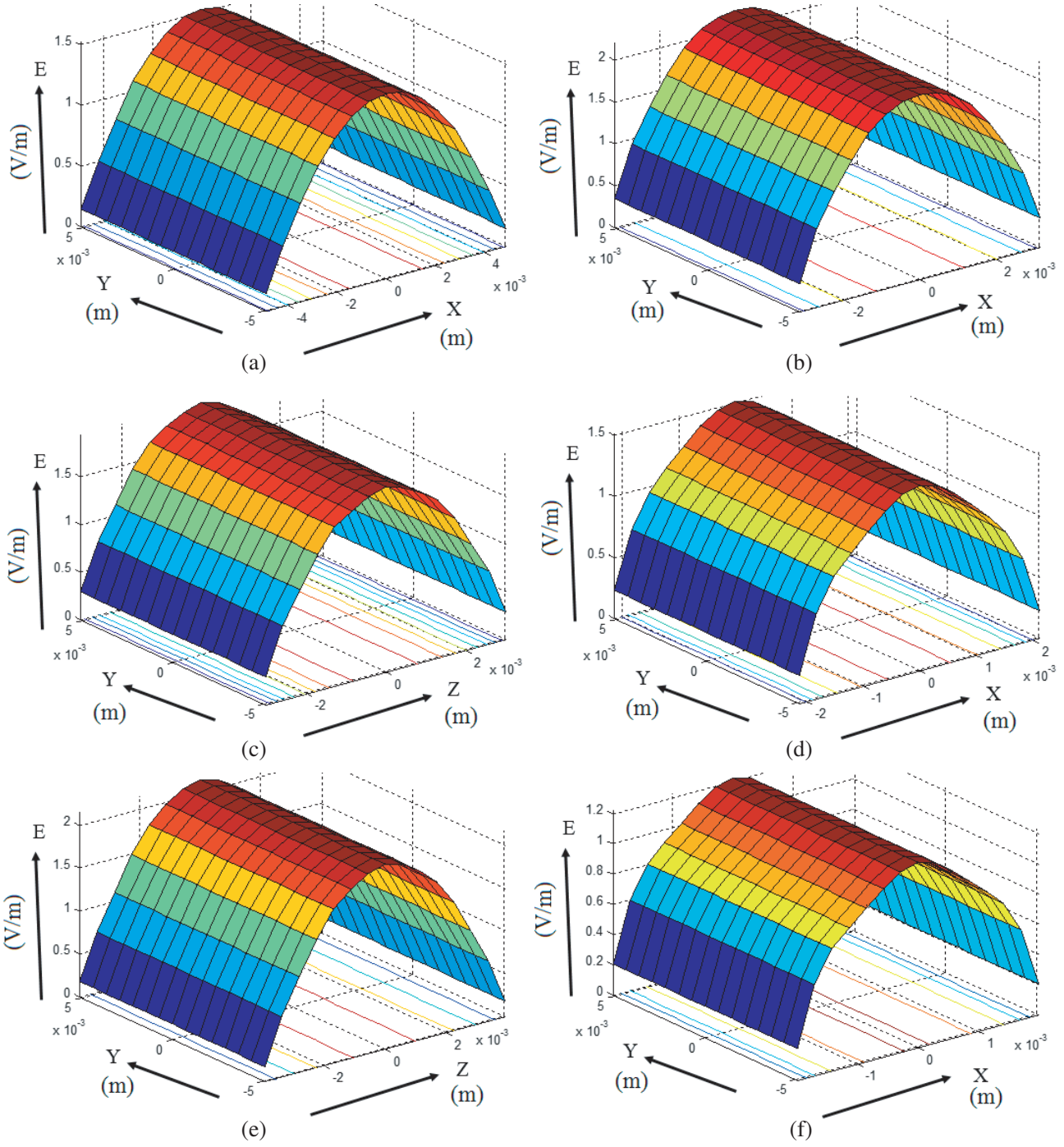

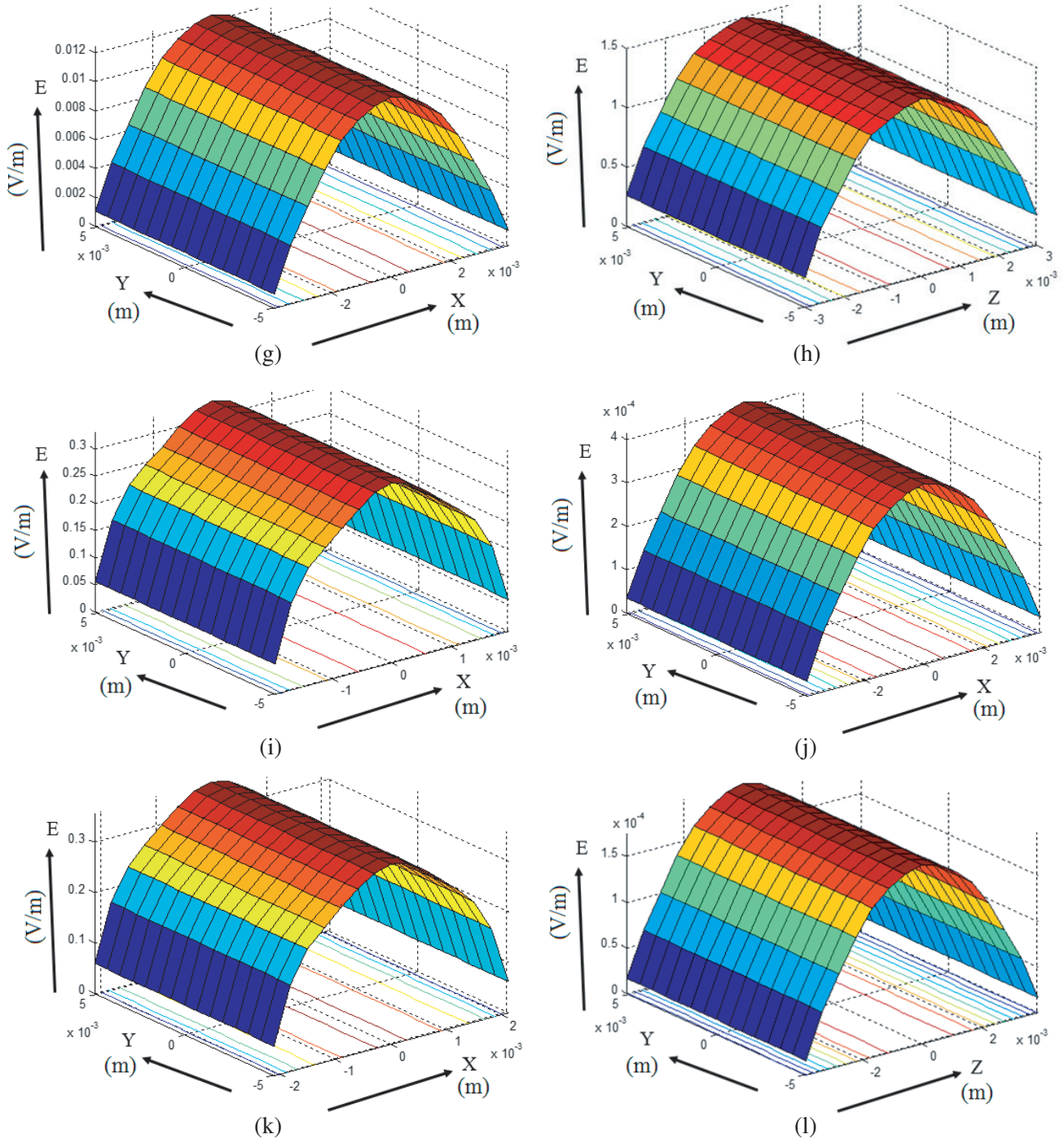

Figure 3. Aperture field distributions on (a) Aperture 1, (b) Aperture 4, (c) Aperture 5, (d) Aperture 7, (e) Aperture 14, (f) Aperture 15, (g) Aperture 22, (h) Aperture 23, (i) Aperture 25, (j) Aperture 32, (k) Aperture 33, and (l) Aperture 40 of the quadraplexer at 9.895 GHz.

all the output ports.

To analyze the field propagation through a passband channel and a stopband channel, the aperture field distributions at different apertures of the respective channel filters are shown in Figs. 8 and 9 at 9.895 GHz. Fig. 8 reveals that at different points of the passband channel the field remains more or less uniform whereas Fig. 9 reveals that the field continuously decays as it propagates through the stopband

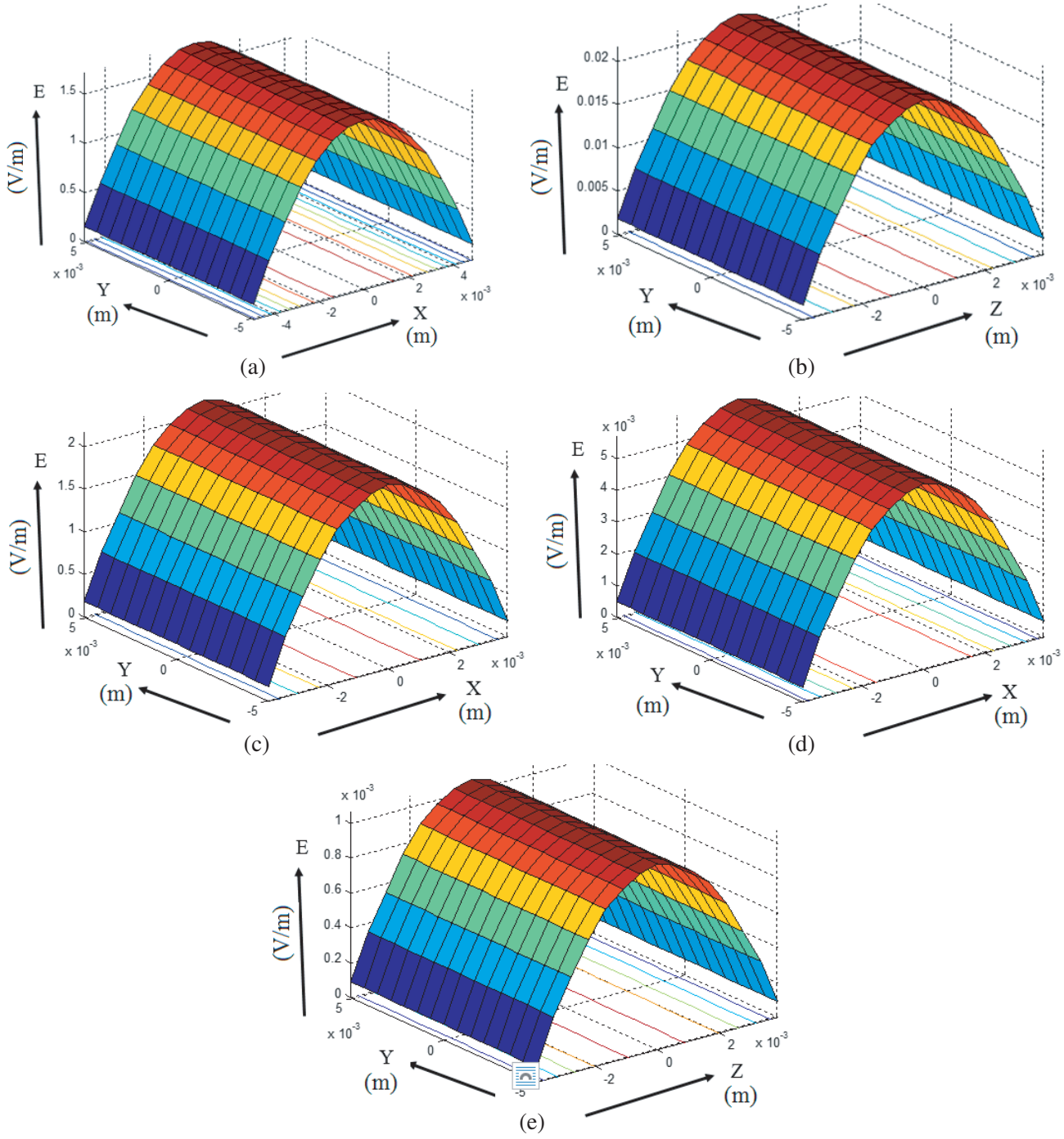

Figure 4. Aperture field distributions on (a) Aperture 1, (b) Aperture 14, (c) Aperture 22, (d) Aperture 32, and (e) Aperture 40 of the quadraplexer at 9.97 GHz.

channel, and at the output port it becomes very weak.

In order to verify the above field propagation and analysis, the frequency response of the quadraplexer has been found and compared with the frequency response available in the literature [8]. The comparison is shown in Fig. 10. The figure reveals close agreement between the simulated and literature available data, which validates the analysis.

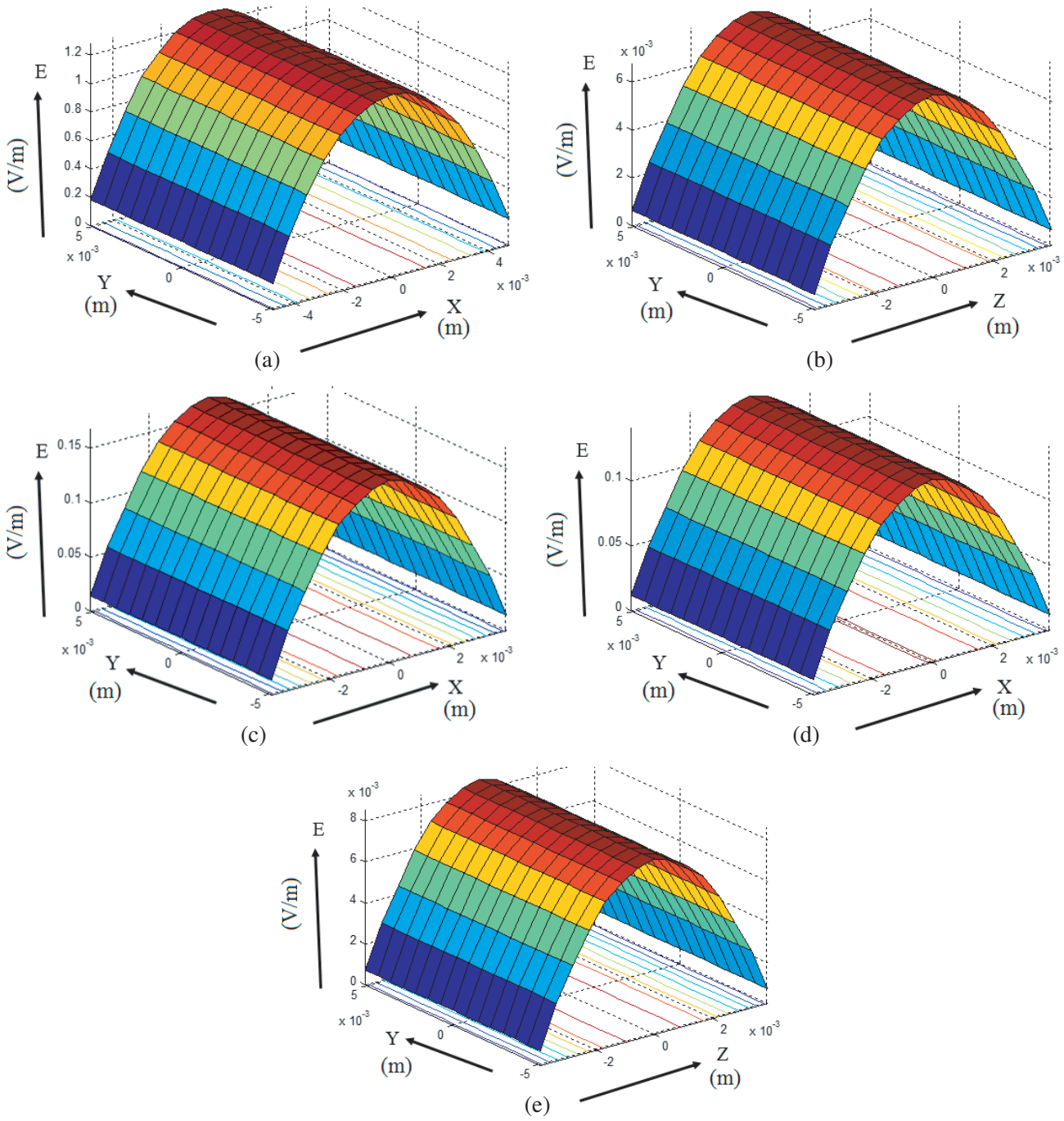

Figure 5. Aperture field distributions on (a) Aperture 1, (b) Aperture 14, (c) Aperture 22, (d) Aperture 32, and (e) Aperture 40 of the quadraplexer at 10 GHz.

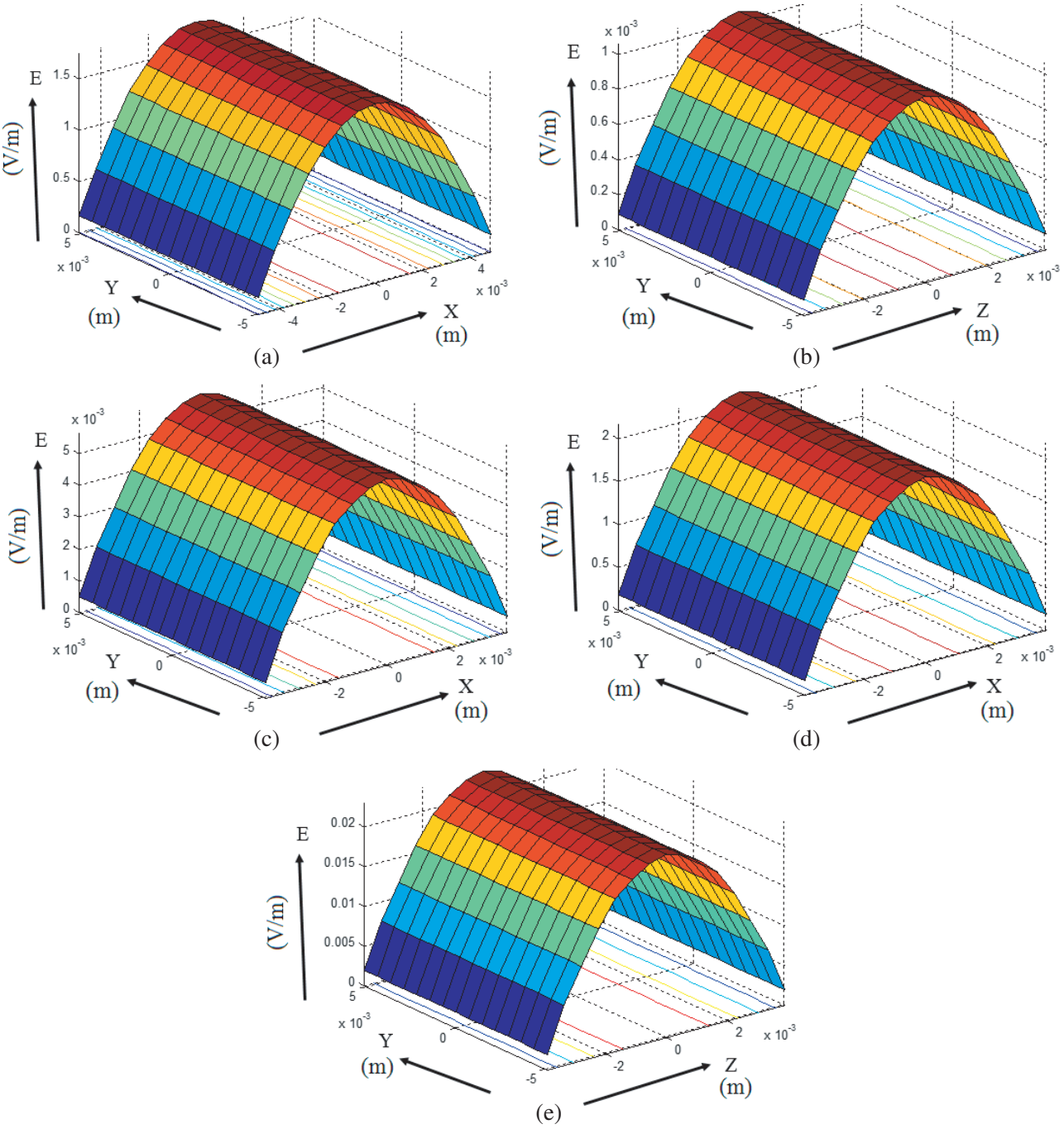

Figure 6. Aperture field distributions on (a) Aperture 1, (b) Aperture 14, (c) Aperture 22, (d) Aperture 32, and (e) Aperture 40 of the quadraplexer at 10.035 GHz.

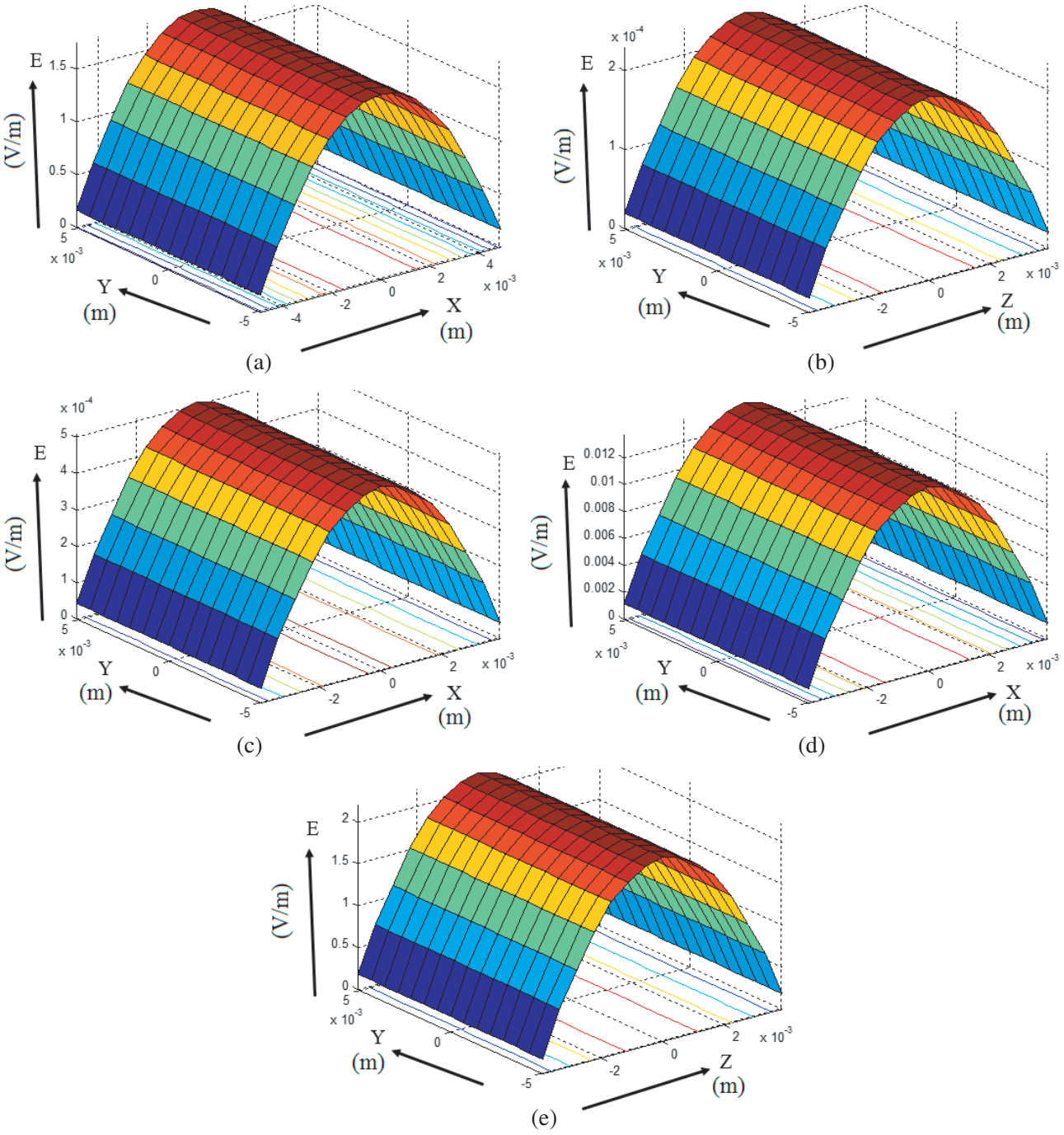

Figure 7. Aperture field distributions on (a) Aperture 1, (b) Aperture 14, (c) Aperture 22, (d) Aperture 32, and (e) Aperture 40 of the quadraplexer at 10.11 GHz.

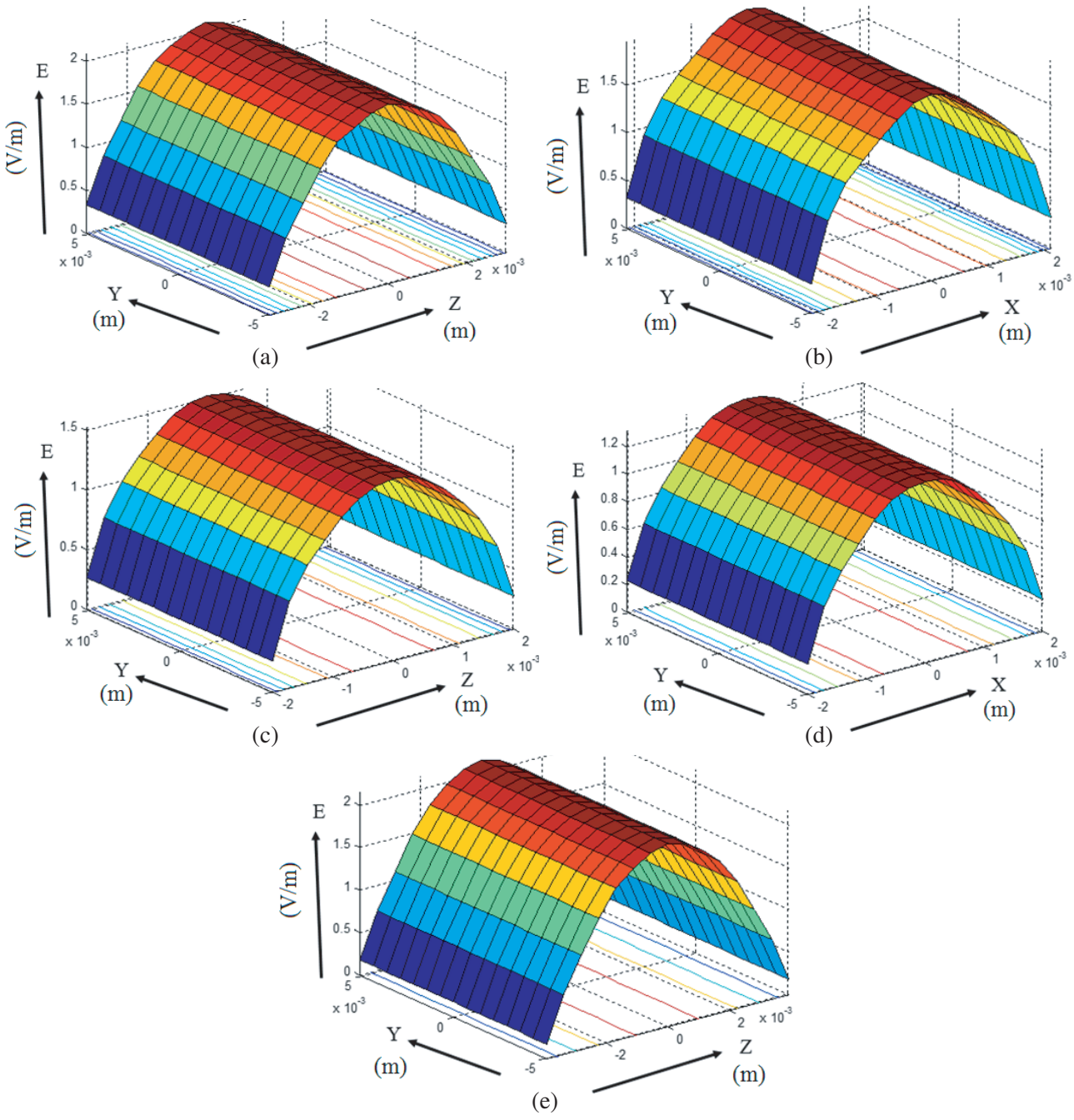

Figure 8. Propagation of field through a passband channel (or channel filter 1) at 9.895 GHz. (a) Aperture 6, (b) Aperture 8, (c) Aperture 10, (d) Aperture 12, and (e) Aperture 14.

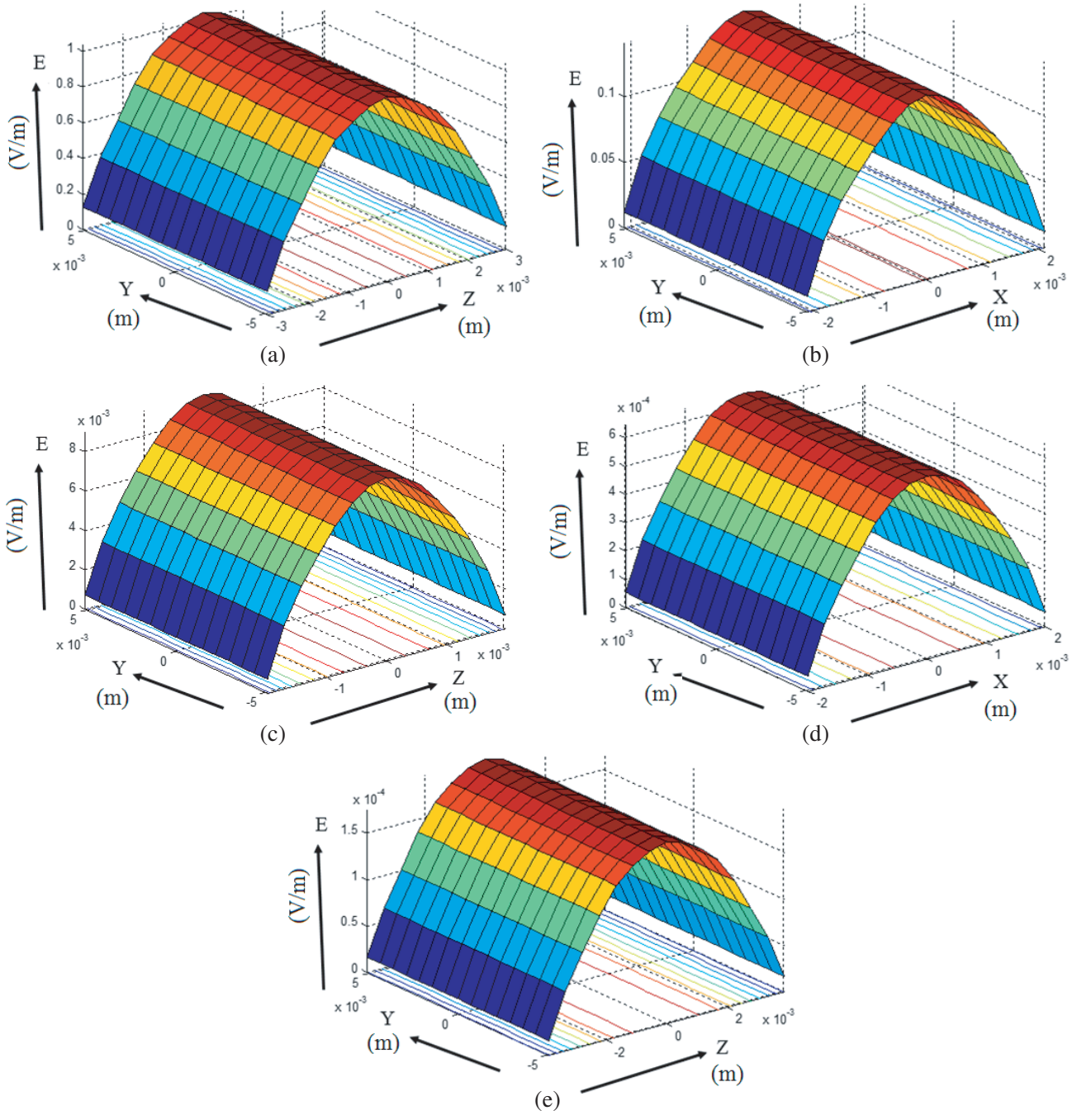

Figure 9. Propagation of field through a stopband channel (or channel filter 4) at 9.895 GHz. (a) Aperture 24, (b) Aperture 34, (c) Aperture 36, (d) Aperture 38, and (e) Aperture 40.

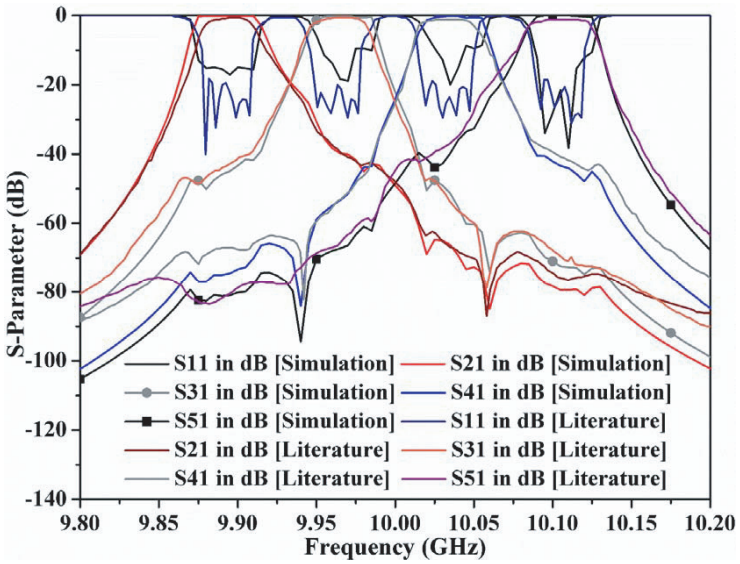

Figure 10. Comparison of the frequency response of the quadraplexer with literature available data [8].

4. CONCLUSION

In this paper, the cavity modeling technique has been successfully applied to analyze the field propagation inside a multiport frequency selective waveguide network. Three-dimensional electric field distributions on different ports, apertures and junctions of the network at different passband and stopband frequencies have been plotted and analyzed. The plots demonstrate field division at different junctions as well as field attenuation/propagation at different points of the network. The analysis has been verified by comparing the overall frequency response of the network with the data available in the literature. The plotted aperture field distributions reveal the propagation of dominant TE_{10} mode. The minor deviations of the aperture field distributions from the exact dominant TE_{10} mode shape at a few junctions/apertures indicate the presence of higher order modes at the discontinuities.

The presented work extends the applicability of cavity modeling technique in analyzing complex multi-port frequency selective waveguide networks and makes the technique more generalized. It enables the determination of 3D field distribution at an arbitrary plane of the network. The 3D field distribution can be used to estimate and determine the higher order modes present in the aperture, if any. The presence of higher order modes often degrade the performance of a network. Therefore by analyzing the field distribution and taking suitable measure to reduce these higher order modes, performance of a network can be improved.

A lot of commercially available software can be used to simulate microwave networks. However, accuracy of the results obtained from the software depends on the settings of different parameters in the software, such as radiation boundary, number of passes, meshing criteria, port definition, module and solver selection, and a wrong setting of any one of them may give erroneous result. In addition, the software is very costly and cannot be afforded by all. It is not applicable in the case of mathematical modeling of RF components. So the researchers, who have limited financial resource but still want a generalized method to simulate different waveguide based networks with a good accuracy, can use cavity modeling technique for this purpose.

ACKNOWLEDGMENT

The authors would like to thank Dr. Sushrut Das, Associate Professor, Department of Electronics Engineering, Indian Institute of Technology (Indian School of Mines) Dhanbad for his suggestions during this work.

REFERENCES

1. Das, S. and A. Chakraborty, "A novel modeling technique to solve a class of rectangular waveguide based circuits and radiators," *Progress In Electromagnetic Research*, Vol. 61, 231–252, May 2006.
2. Das, S., A. Chakraborty, and A. Chakraborty, "Characteristics of an offset longitudinal/transverse slot coupled crossed waveguide junction using multiple cavity modeling technique considering the TE_{00} mode at the slot aperture," *Progress In Electromagnetic Research*, Vol. 67, 297–316, January 2007.
3. Das, S. and A. Chakraborty, "Applicability of multiple cavity modeling technique on electrically large structures," *Journal of Electromagnetic Waves and Application*, Vol. 22, No. 4, 483–492, 2008.
4. Panda, D. K. and A. Chakraborty, "Multiple cavity modeling of a feed network for two dimensional phased array application," *Progress In Electromagnetic Research Letters*, Vol. 2, 135–140, 2008.
5. Panda, D. K., A. Chakraborty, and S. R. Choudhury, "Analysis of co-channel interference at waveguide joint using multiple cavity modelling technique," *Progress In Electromagnetic Research Letters*, Vol. 4, 91–98, 2008.
6. Gayen, R. K. and S. Das, "A high-gain broad-band waveguide longitudinal slot array antenna," *Progress In Electromagnetic Research C*, Vol. 44, 239–249, 2013.
7. Vengadarajan, A., "Multiple cavity modeling technique for solving aperture coupled waveguide junctions," Ph.D. Dissertation, Department of Electronics & Electrical Communication Engineering, Indian Institute of Technology, Kharagpur, India, 1999.
8. Shang, X., Y. Wang, W. Xia, and M. J. Lancaster, "Novel multiplexer topologies based on all-resonator structure," *IEEE Transactions on Microwave Theory and Techniques*, Vol. 61, No. 11, 3838–3844, November 2013.
9. Harrington, R. F., *Time-Harmonic Electromagnetic Fields*, McGraw-Hill Book Company, New York, 1961.